PHYSICAL ORIGIN OF THE TRANSITION FROM SYMMETRIC TO ASYMMETRIC FISSION FRAGMENT CHARGE DISTRIBUTION*

H. Pașca[a,b], A.V. Andreev[a], G.G. Adamian[a], N.V. Antonenko[a,c]

[a]Joint Institute for Nuclear Research, 141980 Dubna, Russia
[b]Babeş-Bolyai University, 400084 Cluj-Napoca, Romania
[c]Mathematical Physics Department, Tomsk Polytechnic University
634050 Tomsk, Russia

(Received December 14, 2016)

Using the improved scission-point model, the isotopic trends of the charge distribution of fission fragments are studied in induced fission of even–even Th isotopes at low- and high-excitation energies.

DOI:10.5506/APhysPolB.48.431

1. Introduction

A longstanding question is how and why the transition occurs from symmetric to asymmetric fission mode. As known, the experimental [1] charge distributions in the electro-magnetic-induced fission ($E_\gamma = 11$ MeV) of even–even isotopes ^{218,220,222}Th are clearly symmetric, with one relatively narrow peak. For ^{224}Th, the distribution starts showing the formation of two asymmetric peaks, while for the ^{226}Th, the yields around Kr–Sr and their complementary fragments are equal to those around Pd–Ru. As the mass number of the Th increases to $A = 228$, the symmetric peak recedes and the asymmetric mode becomes dominant. Thus, with the increasing neutron number, the transition from one-peaked to two-peaked charge distribution occurs through transient three-peaked shape in which the symmetric and asymmetric components of the distribution have almost equal weights. Our aim is to explain this transformation of the charge distribution with neutron number, from ^{218}Th to ^{228}Th, at 11 MeV excitation energy and to predict the charge distributions at large excitation energies. One of other motivating factors of our work is the general opinion that at high-excitation energies

* Presented by G.G. Adamian at the Zakopane Conference on Nuclear Physics "Extremes of the Nuclear Landscape", Zakopane, Poland, August 28–September 4, 2016.

the charge/mass distributions should all be symmetric, while the experiment [2] showed that for ^{238}U(n,f), the asymmetric shape is conserved even at 60 MeV neutron energy.

In the present paper, the origin of the evolution of the charge distribution with increasing neutron number is studied within the scission-point model [3, 4]. The most important ingredient of the model is the potential energy of system as a function of charge (mass) asymmetry, deformations of the fission fragments, and internuclear distance. The knowledge of the deformations of nascent fragments at scission point is also crucial. The distance between the tips of the fission fragments at scission and the excitation energy are not the parameters of our model but are defined from the potential energy.

2. Scission-point model

The statistical scission-point model relies on the assumption that the statistical equilibrium is established at scission where the observable characteristics of fission process are formed. The dinuclear system (DNS) model [3, 4] is shown to be well-suited for describing the scission configuration. The fissioning nucleus at scission point is modeled by two nearly touching coaxial ellipsoids — fragments of the DNS with masses (charges) numbers $A_{\rm L}$ ($Z_{\rm L}$) and $A_{\rm H}$ ($Z_{\rm H}$) for the light (L) and heavy (H) fragments, respectively. Here, $A = A_{\rm L} + A_{\rm H}$ ($Z = Z_{\rm L} + Z_{\rm H}$) is the mass (charge) number of fissioning nucleus. By taking into consideration the volume conservation, the shape of the system is defined by the mass and charge numbers of the fragments, deformation parameters of fragments, β_i ($i = {\rm L}, {\rm H}$), and interfragment distance R. The index i designates the light or heavy fragment of the DNS. The potential energy [4]

$$\begin{aligned} U(A_i, Z_i, \beta_i, R) \;=\; & U_{\rm L}^{\rm LD}\left(A_{\rm L}, Z_{\rm L}, \beta_{\rm L}\right) + \delta U_{\rm L}^{\rm shell}\left(A_{\rm L}, Z_{\rm L}, \beta_{\rm L}, E_{\rm H}^{*}\right) \\ & + U_{\rm H}^{\rm LD}\left(A_{\rm H}, Z_{\rm H}, \beta_{\rm H}\right) + \delta U_{\rm H}^{\rm shell}\left(A_{\rm H}, Z_{\rm H}, \beta_{\rm H}, E_{\rm H}^{*}\right) \\ & + V^{\rm C}\left(A_i, Z_i, \beta_i, R\right) + V^{\rm N}\left(A_i, Z_i, \beta_i, R\right) \end{aligned} \tag{1}$$

of the DNS consists of the energies of the fragments and energy $V^{\rm C} + V^{\rm N}$ of their interaction. The nuclei in the DNS have the excitation energies E_i^*. The energy of each fragment consists of the excitation-energy-dependent liquid-drop energy $U_i^{\rm LD}$ and deformation-dependent shell-correction term $\delta U_i^{\rm shell}$ calculated with the Strutinsky method and the two-center shell model. The damping of the shell corrections with excitation energy E_i^* is introduced as $\delta U_i^{\rm shell}(A_i, Z_i, \beta_i, E_i^*) = \delta U_i^{\rm shell}(A_i, Z_i, \beta_i, E_i^* = 0) \exp[-E_i^*/E_{\rm D}]$, where $E_{\rm D} = 18.5$ MeV is the damping constant. The interaction potential consists of the Coulomb interaction potential $V^{\rm C}$ of the two uniformly charged ellipsoids and nuclear interaction potential $V^{\rm N}$ in the double-folding form [3, 4].

The interaction potential has a potential pocket with external barrier located at the distances between the tips of the fragments of about (0.5–1) fm and (1.5–2) fm [in the considered region of fission fragments], respectively, depending on deformations of the fragments. The internuclear distance R in Eq. (1) corresponds to the position $R = R_m(A_i, Z_i, \beta_i)$ of the minimum of this pocket. The barrier, $B_{qf}(A_i, Z_i, \beta_i)$, calculated as the difference of the potential energies at the bottom of the potential pocket $[R = R_m(A_i, Z_i, \beta_i)]$ and at the top of the external barrier $[R = R_b(A_i, Z_i, \beta_i)]$, prevents the decay of the DNS in R. Note that the height of the barrier decreases with charge asymmetry.

Because the thermal equilibrium is assumed at scission point, the excitation energy $E^*(A_i, Z_i, \beta_i, R_m)$ at scission is calculated as the initial excitation energy of fissioning nucleus $E^*_{\rm CN}$ plus the difference between the potential energies of fissioning nucleus $U_{\rm CN}(A, Z, \beta)$ and of the system at the scission point $U(A_i, Z_i, \beta_i, R_m)$ [4]: $E^*(A_i, Z_i, \beta_i, R_m) = E^*_{\rm CN} + [U_{\rm CN}(A, Z, \beta) - U(A_i, Z_i, \beta_i, R_m)]$. The relative formation probability of the DNS with particular masses, charges and deformations of the fragments is statistically calculated as follows:

$$w(A_i, Z_i, \beta_i, E^*) = N_0 \exp\left[-\frac{U(A_i, Z_i, \beta_i, R_m) + B_{qf}(A_i, Z_i, \beta_i)}{T}\right], \quad (2)$$

where N_0 is the normalization factor. The ratio of the yields of fragments with different charge/mass numbers is mainly governed by the difference in energy between the corresponding potential minima in the plane $(\beta_{\rm L}, \beta_{\rm H})$, as seen in Eq. (2). For the two potential energy surfaces with minima, which are close in energy, a higher yield stems from the DNS with a wider and shallower minimum, and lower yield emerges from an abrupt and narrow minimum. In Eq. (2), the temperature is calculated as $T = \sqrt{E^*/a}$, where $a = A/12$ MeV^{-1} is the level density parameter in the Fermi-gas model. In our calculations, a single value is used for the temperature at the global potential minimum of U before the shell damping. As seen, the height B_{qf} of the decay barrier has also an impact on the yields. With increasing elongation and decreasing charge (mass) asymmetry the value of B_{qf} decreases, the system becomes more unstable and decays.

In order to obtain the charge distribution of fission fragments, one should integrate (2) over $\beta_{\rm L}$ and $\beta_{\rm H}$, and sum over A_i:

$$\begin{aligned} Y(Z_i, E^*) &= \frac{\sum_{A_i} Y(A_i, Z_i, E^*)}{\sum_{Z_i, A_i} Y(A_i, Z_i, E^*)}, \\ Y(A_i, Z_i, E^*) &= N_0 \int {\rm d}\beta_{\rm L}\, {\rm d}\beta_{\rm H} w(A_i, Z_i, \beta_i, E^*). \end{aligned} \quad (3)$$

Because the dynamical treatment is not explicitly performed here, we simulate the dynamical effects by restricting the minimum value of the barrier B_{qf}. In the calculations, we take into consideration only those configurations for which B_{qf} is larger than ~ 1 MeV. This condition restricts the highly deformed unstable configurations in the (β_{L}, β_{H}) plane and, correspondingly, restricts the upper limits of integration over deformations $\beta_{\mathrm{L,H}}$. As shown below, the experimental data are described well with this restriction.

3. Calculated results

The experimental [1] and calculated charge distributions resulted from the electro-magnetic-induced ($E_\gamma = 11$ MeV) fission of even–even nuclei $^{204-208}$Rn, $^{210-218}$Ra, $^{218-228}$Th, and $^{230-234}$U are shown in Figs. 1–3. As seen, our model is suitable for describing both symmetric and asymmetric charge distributions, and shows a good agreement with the experimental data.

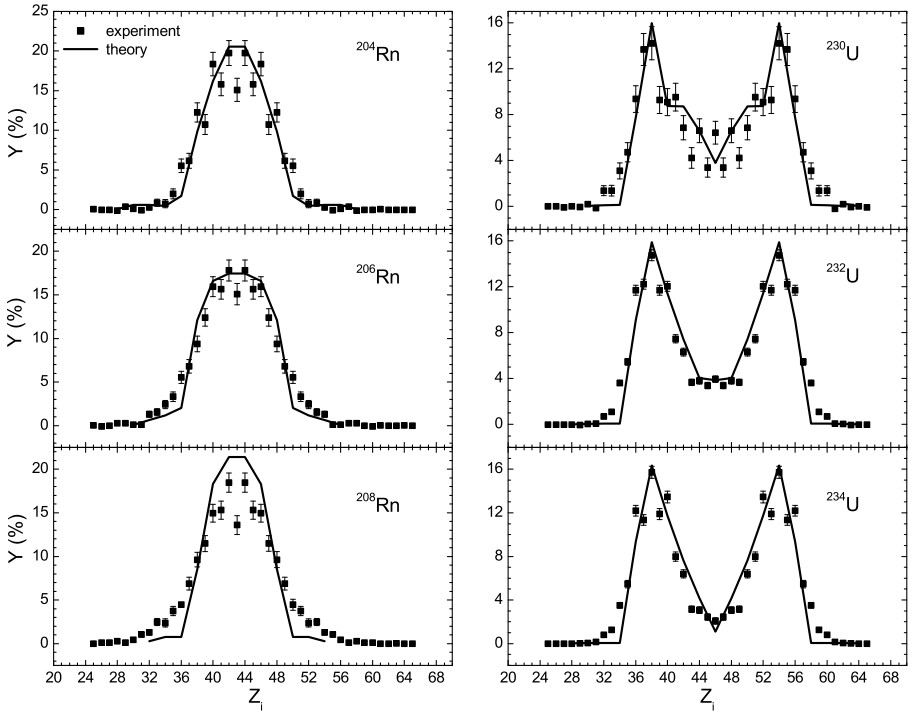


Fig. 1. The calculated charge distributions (lines) for electro-magnetic-induced fission of the indicated radon and uranium isotopes at 11 MeV excitation energy are compared with the experimental data [1] (symbols). The lines connect the calculated points for even–even fission fragments.

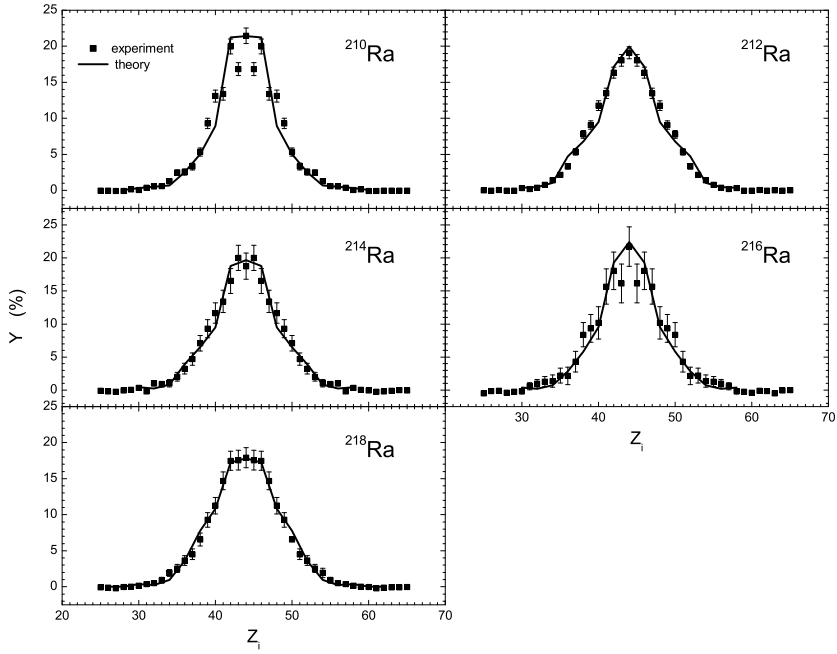


Fig. 2. The same as in Fig. 1, but for the indicated radium isotopes.

For the Th isotopes, the transition from one-peaked to two-peaked distribution, going through transient three-peaked shape can be explained by studying the driving potential $U(Z_i) = U(A_i, Z_i, \beta_i, R_m)$ of the system [Eq. (1)]. Here, the values A_i and β_i are related to Z_i to supply the minimum of U. In the case of ^{218,220,222}Th isotopes, the driving potential $U(Z_i)$ shows a deep minimum at $Z/2 = 45$ (Fig. 4). For the ^{224}Th nucleus, $U(Z_i)$ starts displaying the formation of the second minimum around Kr–Sr, while for the ^{226}Th isotope, the second minimum becomes almost as deep as the central (symmetric) one. Even though the values of $U(Z_\mathrm{L} = 36\text{–}38)$ are higher by about 0.5 MeV than $U(Z/2)$, the corresponding yields are the same. This is easily explained by the fact that in $(\beta_\mathrm{L}, \beta_\mathrm{H})$ plane, the minima for Kr–Sr are wider than those for Ru–Pd. For the ^{228}Th nucleus, the asymmetric minima become deeper, facilitating the asymmetric fragmentation, but the central minimum still remains.

To understand the conditions under which the mass-asymmetric minimum appears in the driving potential, one can analyze the components of the driving potential: the liquid-drop energy $U^\mathrm{LD} = U^\mathrm{LD}_\mathrm{L} + U^\mathrm{LD}_\mathrm{H}$, the interaction potential $V = V^\mathrm{C} + V^\mathrm{N}$, and the shell-correction energy $\delta U^\mathrm{shell} = \delta U^\mathrm{shell}_\mathrm{L} + \delta U^\mathrm{shell}_\mathrm{H}$ (Fig. 5). The absolute value of δU^shell is much smaller than the values of U^LD and V. The U^LD increases globally when the charge

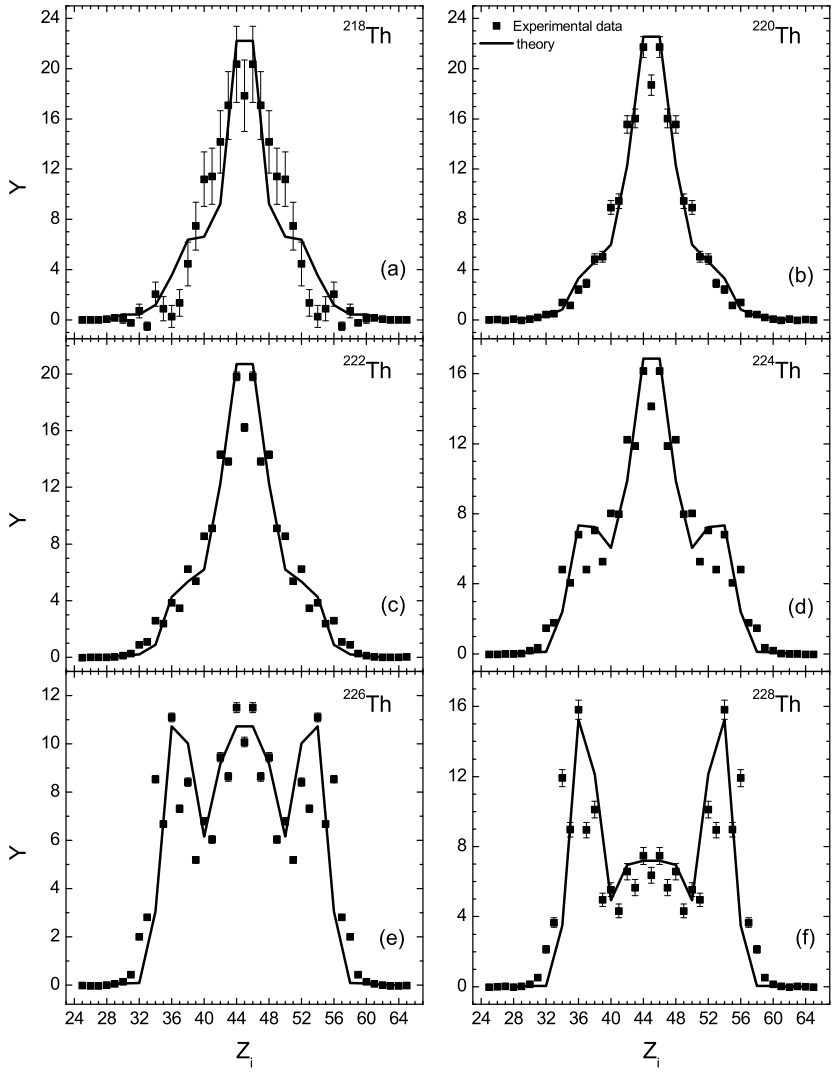


Fig. 3. The same as in Fig. 1, but for the indicated thorium isotopes.

(mass) number deviates from $Z/2$ ($A/2$). The V has the opposite global behavior. On the other side, both components of the driving potential depend on deformations of the DNS nuclei, which creates local minima in the $U^{\mathrm{LD}}(Z_i)$ and $V(Z_i)$. The higher deformations lead to the smaller V and the larger U^{LD}. The deformations [the positions of minima in the (β_{L}, β_{H}) plane] depend on the shell corrections. The strong shell effects in semi-magic and almost semi-magic nuclei with $Z_{\mathrm{L}} < 40$ are expressed in the relatively small deformations of the corresponding nuclei. For the nuclei with charge

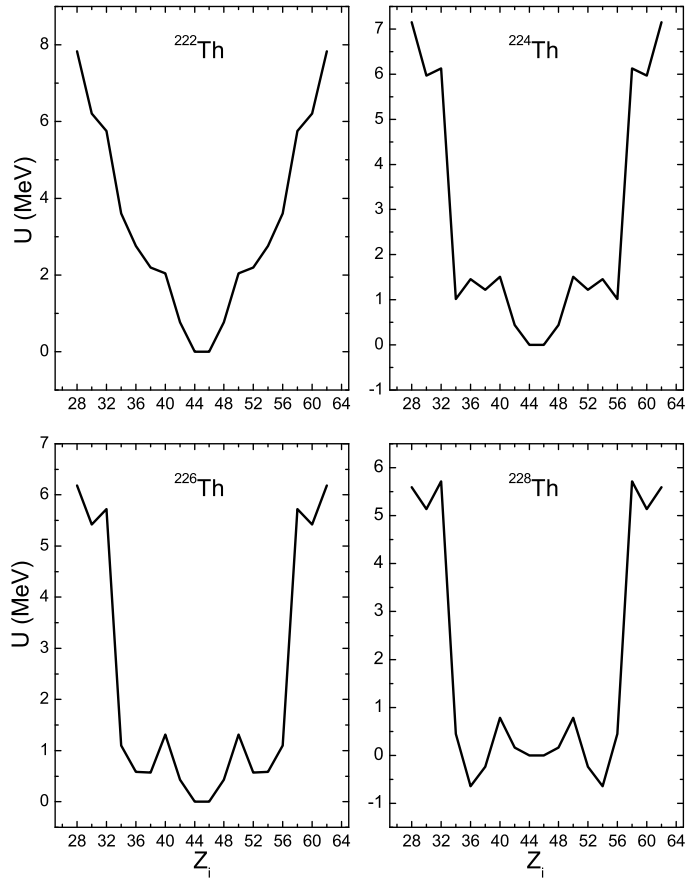


Fig. 4. The calculated driving potentials for indicated thorium isotopes. The potentials are normalized to the energy $U(Z_{\rm L} = 44) = 0$ MeV. The values of A_i and β_i are related to Z_i to supply the minimum of U.

numbers larger than $Z_{\rm L} = 40$, the shell effects are almost negligible, as $Z_{\rm L}$ ($N_{\rm L}$) are midway between proton (neutron) numbers of the closed shells. This leads to an almost pure liquid-drop behavior of the system that causes higher deformations of the fragments. Thus, the asymmetric minimum in the driving appears due to the competition of the liquid-drop energy and the nucleus–nucleus interaction potential. The shell corrections affect indirectly (through the deformations of nuclei) on the appearance of the asymmetric minimum and directly by changing the position and depth of this minimum. For example, for ^{224}Th (Fig. 5) at $Z_{\rm L} = 34$, 36 and 38, the nuclei are very close to the $N_{\rm L} = 50$ and $N_{\rm H} = 82$ shells, which means high value of the stiffness parameter with respect to the change of deformation. As a result, at $Z_{\rm L} = 34$–38, the V decreases faster than the $U^{\rm LD}$ increases, at $Z_{\rm L} < 34$,

the increase of the U^{LD} quickly dominates over the decrease of the V and, at $Z_{\mathrm{L}} = 34$, the asymmetric minimum is produced. The shell corrections decrease the depth of this minimum.

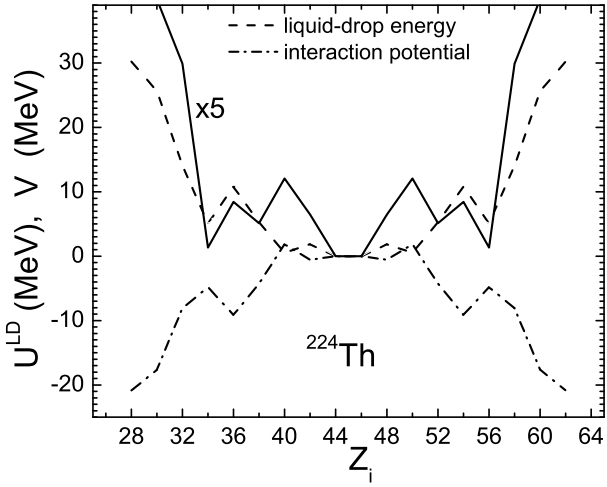


Fig. 5. The calculated components U^{LD} (dashed line) and V (dash-dotted line) of the driving potential at 11 MeV excitation energy for indicated fissioning nucleus. The U^{LD}, V, and their sum $U^{\mathrm{LD}} + V$ (solid line) are normalized to the zero energy at $Z_{\mathrm{L}} = 44$. The values of $U^{\mathrm{LD}} + V$ are scaled by a factor 5.

With increasing N–Z of the fissioning nucleus, the liquid-drop energy (interaction potential) increases slower (faster) with charge asymmetry. This is the reason of the appearance of the pronounced asymmetric minimum in the cases of ^{226,228}Th.

In Fig. 6, the charge distributions of fissioning nuclei ^{222,224,226,228}Th at 35 and 60 MeV excitation energies are predicted. In all four cases, the distribution widens with excitation energy. For ^{222,224}Th isotopes [Fig. 6 (a) and (b)], the central peak recedes, and two asymmetric peaks appear suppressing the symmetric mode. The charge distributions of ^{226,228}Th at higher excitation energies [Fig. 6 (c) and (d)] emphasize the asymmetric aspect of the distribution, making the symmetric peak smaller and narrower, and the asymmetric maxima wider and taller. This is easily explained by the fact that with higher excitation energy, the previously unaccessible asymmetric configurations are involved. With increasing excitation energy of the fissioning nucleus, the liquid-drop energy U^{LD} (or the liquid-drop surface energy) increases slower with charge asymmetry. This leads to the pronounced asymmetric minimum in the cases of ^{222,224}Th.

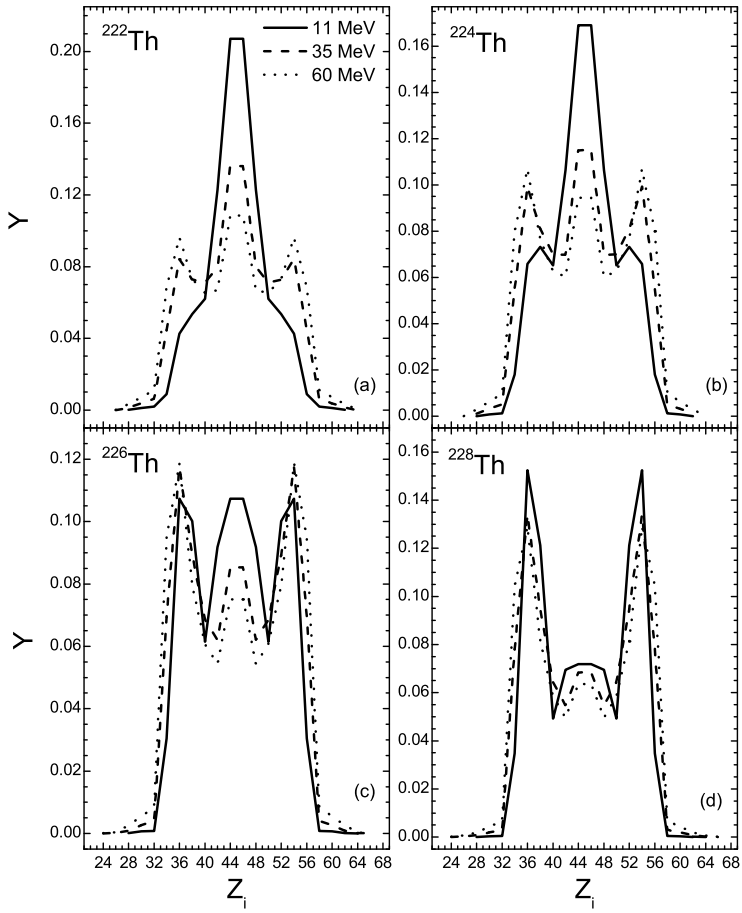


Fig. 6. The predicted charge distributions for ^{222,224,226,228}Th isotopes at 11, 35, and 60 MeV excitation energies of the initial compound nucleus. The lines connect the calculated yields of even–even fission fragments.

4. Conclusions

The improved scission-point model provides a good description of the charge distributions of low-energy fission of even–even nuclei $^{204-208}$Rn, $^{210-218}$Ra, $^{218-228}$Th, and $^{230-234}$U. For the fission of Th isotopes, we described the transformation of the shape of charge distribution from symmetric to asymmetric with increasing mass of fissioning nucleus. These one-, two- or three-peaked charge distributions were explained with the driving potentials of these systems at the scission point. The competition between the liquid-drop surface energy and the nucleus–nucleus interaction potential is one of the main reasons of the appearance or disappearance of the asymmetric fission mode.

From our calculations, we concluded that the three-equal-peaked charge distribution is not the specific property of the ^{226}Th nucleus. The shape of the charge distribution depends on the excitation energy. For the fissioning nucleus ^{226}Th at high excitation energies, the charge distributions are asymmetric but not the three-equal-peaked ones. We predicted the appearance of the three-equal-peaked charge distributions for the fissioning nuclei ^{222}Th and ^{224}Th at about 60 MeV and 35–60 MeV excitation energies, respectively. The experimental verification of this effect is desirable.

REFERENCES

[1] K.-H. Schmidt *et al.*, *Nucl. Phys. A* **665**, 221 (2000); **693**, 169 (2001).
[2] I.V. Ryzhov *et al.*, *Phys. Rev. C* **83**, 054603 (2011).
[3] H. Paşca *et al.*, *Phys. Rev. C* **93**, 054602 (2016).
[4] H. Paşca *et al.*, *Phys. Lett. B* **760**, 800 (2016).